

A 20 year-long GNSS solution across South-America with focus in Chile

Emilie Klein, Christophe Vigny, Jean-Mathieu Nocquet, Hugo Boulze

▶ **To cite this version:**

Emilie Klein, Christophe Vigny, Jean-Mathieu Nocquet, Hugo Boulze. A 20 year-long GNSS solution across South-America with focus in Chile. Bulletin de la Société Géologique de France, 2022, 193, pp.5. 10.1051/bsgf/2022005 . hal-03711841

HAL Id: hal-03711841
https://hal.science/hal-03711841

Submitted on 1 Jul 2022

HAL is a multi-disciplinary open access archive for the deposit and dissemination of scientific research documents, whether they are published or not. The documents may come from teaching and research institutions in France or abroad, or from public or private research centers.

L'archive ouverte pluridisciplinaire **HAL**, est destinée au dépôt et à la diffusion de documents scientifiques de niveau recherche, publiés ou non, émanant des établissements d'enseignement et de recherche français ou étrangers, des laboratoires publics ou privés.

BSGF - Earth Sciences Bulletin 2022, 193, 5
© E. Klein *et al.*, Published by EDP Sciences 2022
https://doi.org/10.1051/bsgf/2022005

BSGF
Earth Sciences Bulletin
Available online at:
www.bsgf.fr

Open Access

A 20 year-long GNSS solution across South-America with focus in Chile

Emilie Klein[1], Christophe Vigny[1], Jean-Mathieu Nocquet[2,3] and Hugo Boulze[1]

[1] Laboratoire de Géologie – CNRS UMR 8538, École normale supérieure – PSL University, Paris, France
[2] Université de Paris, Institut de Physique du Globe de Paris, CNRS, 75005 Paris, France
[3] Université Côte d'Azur, IRD, CNRS, Observatoire de la Côte d'Azur, Géoazur, 250 rue Albert Einstein, Sophia Antipolis, 06560 Valbonne, France

Received: 25 November 2021 / Accepted: 22 January 2022 / Publishing online: 21 June 2022

Abstract – Over the last 3 decades, GPS measurements have been instrumental in quantifying tectonic plates current motion and deformation. Complex patterns of deformation along the plate boundaries revealed heterogeneous coupling on the plates interface and imaged seismic segments at different stages of their seismic cycle. Along the South-American trench in Chile, where large earthquakes occur frequently, continuous GPS observations (cGPS) captured both the long-term plate motion and the transient deformations associated with the seismic cycle. Over the years, a network of hundreds of cGPS stations has been deployed all across the South-American continent by many different institutions for many different sorts of purposes ranging from geographic reference to tsunami early warning. We report here on the processing of 20 years (2000–2020) worth of data over a selection of cGPS stations, devoted to the quantification and analysis of the deformation along the Chilean subduction zone between 18°S and 40°S. We use all available data near the trench in Chile and a less dense network inside the continent where the gradient of deformation is lesser. Our database, named *SOAM_GNSS_solENS*, provides time series of precise daily station position, obtained from double difference (DD) processing and expressed in the International Terrestrial Reference Frame 2014 (ITRF14). These time series allow to quantify, with sub-millimetric precision, any kind of ongoing deformation process, either from tectonic origin such as interseismic deformation, co- and post-seismic displacements associated with earthquakes, transient deformation associated to seismic swarms and/or a-seismic slow-slip events, or of other origin such as hydrological loading (for ex., the Amazonian basin load) or any other type of loading affecting the surface of the Earth (tides, atmosphere, etc.). We also provide a database of coseismic displacements associated with close to 60 earthquakes of Mw larger than 6.5 that occurred over the last 20 years within the observation area. All time series are directly accessible through a deposit and we plan to make them available through a web interface that will allow any user to perform elementary operations like estimating offsets, detecting outliers, detrending, filtering and stacking. That database will evolve with time, aggregating more data. In the future, we also plan to complement that database with a rapid solution in quasi real time processed in Precise Point Positioning (PPP), and with hourly atmospheric delays associated with water vapor content of the lower layer of the atmosphere.

Keywords: GNSS solution / South America / Chile / subduction / earthquake

Résumé – Au cours des trois dernières décennies, les mesures GPS ont permis de quantifier le mouvement et la déformation actuelle des plaques tectoniques. Des modèles complexes de déformation le long des frontières des plaques ont révélé un couplage hétérogène à l'interface des plaques, et ont permis d'imager des segments sismiques à différents stades de leur cycle sismique. Le long de la fosse sud-américaine au Chili, où de grands tremblements de terre se produisent fréquemment, des observations GPS continues (cGPS) ont capturé à la fois le mouvement des plaques à long terme et les déformations transitoires associées au cycle sismique. Au fil des ans, un réseau de plusieurs centaines de stations cGPS a été déployé sur tout le continent sud-américain, par de nombreuses institutions différentes, pour toutes sortes d'applications allant

*Corresponding author: klein@geologie.ens.fr

This is an Open Access article distributed under the terms of the Creative Commons Attribution License (https://creativecommons.org/licenses/by/4.0), which permits unrestricted use, distribution, and reproduction in any medium, provided the original work is properly cited.

de la référence géographique à l'alerte précoce aux tsunamis. Nous présentons ici le traitement de 20 années (2000–2020) de données sur une sélection de stations cGPS, consacrées à la quantification et à l'analyse de la déformation le long de la zone de subduction chilienne entre 18°S et 40°S. Nous utilisons toutes les données disponibles au Chili (proche de la fosse de subduction) et un réseau moins dense à l'intérieur du continent où le gradient de déformation est moindre. Notre base de données, nommée *SOAM_GNSS_solENS*, fournit des séries temporelles de position quotidienne précise des stations, obtenues par traitement en double différence (DD) et exprimées dans le système international de référence terrestre 2014 (ITRF14). Ces séries temporelles permettent de quantifier, avec une précision sub-millimétrique, tout type de processus de déformation en cours, qu'il soit d'origine tectonique comme la déformation intersismique, les déplacements co- et post-sismiques associés aux tremblements de terre, la déformation transitoire associée aux essaims sismiques et/ou aux événements de glissement lent a-sismiques, ou d'origine différentes comme les charges hydrologiques (par exemple, la charge du bassin amazonien) ou tout autre type de charge affectant la surface de la Terre (marées, atmosphère, etc.). Nous fournissons également une base de données des déplacements cosismiques associés à près de 60 séismes de Mw supérieure à 6.5, survenus au cours des 20 dernières années dans la zone d'observation et détectés par GPS. Toutes les séries temporelles sont directement accessibles *via* un dépôt et une interface web actuellement en développement permettra à tout utilisateur d'effectuer des opérations élémentaires telles que l'estimation des sauts, la détection des valeurs aberrantes, la correction de tendance linéaire, le filtrage et la superposition. Cette base de données évoluera avec le temps, en agrégeant davantage de données. Dans le futur, nous prévoyons également de la compléter avec une solution rapide en temps quasi réel traitée en Precise Point Positioning (PPP), et avec des séries temporelles de retards atmosphériques horaires associés au contenu en vapeur d'eau de la couche inférieure de l'atmosphère.

Mots clés : solution GNSS / Amérique du Sud / Chili / subduction / séismes

1 Introduction

The Chilean subduction zone is extremely seismically active with on average one Mw 8 earthquake every ten years and at least one mega earthquake of magnitude 9 and over per century (Beck *et al.*, 1998, Lomnitz, 2004, Ruiz and Madariaga, 2018). The largest earthquake ever recorded by seismometers, the 22nd May 1960 Valdivia earthquake of magnitude 9.5, occurred along the southern part of the Chilean subduction zone and generated a giant trans-Pacific tsunami that caused catastrophic damage along the coasts of Hawaii and Japan (Cifuentes, 1989).

Since the early 90's, GPS was instrumental in quantifying details of the tectonic plates motion and deformation in South-America (*e.g.*, Larson *et al.*, 1997, Angermann *et al.*, 1999, Norabuena *et al.*, 1999, Klotz *et al.*, 2001, Kendrick *et al.*, 2001, Ruegg *et al.*, 2002, Kendrick *et al.*, 2003, Brooks *et al.*, 2003, Altamimi *et al.*, 2007). As in many subduction zones worldwide, GPS measurements in Chile showed that the velocity field derived from several years of observation are spatially heterogeneous, drawing large patches where velocity gradient or deformation is intense separated by narrow zones where it is low. Those variations of deformation are evidence of variable coupling along the plate interface, with patches where deformation is high corresponding to long segments of high coupling (*e.g.*, Moreno *et al.*, 2011, Métois *et al.*, 2012, 2016). These segment accumulate deficit of slip and store elastic energy in the surrounding medium, making them prone to a seismic rupture if enough time has elapsed, leading to the concept of seismic gap (*e.g.*, McCann *et al.*, 1979).

In Chile, several of these large seismic gaps ruptured during the last ten years. The Maule earthquake of 27th February 2010 (Mw 8.8), the Iquique earthquake of 1st April 2014 (Mw 8.2) and the Illapel earthquake of 16th September 2015 (Mw 8.4), all occurred in one of these previously identified seismic gaps, where GPS had revealed that deformation was accumulating prior to the earthquake (*e.g.*, Moreno *et al.*, 2010, Vigny *et al.*, 2011, Ruiz *et al.*, 2014, Schurr *et al.*, 2014, Tilmann *et al.*, 2016, Klein *et al.*, 2017). Other identified seismic gaps pause an acute seismic hazard today. The "Great North gap", locus of the megathrust earthquake of 1877 (Comte and Pardo, 1991), the "Atacama gap", locus of the megathrust earthquakes of 1819 and 1922 (Willis, 1929), and the "Valparaiso gap" locus of the 1985 earthquake (Comte *et al.*, 1986), are regions most likely to be approaching the end of their seismic cycle.

GPS, sometimes associated with InSAR, also revealed transient deformation at different time and space scales, associated with seismic swarms and/or a-seismic deformation (Pritchard and Simons, 2006, Klein *et al.*, 2018, Klein *et al.*, 2021) and the post-seismic deformation that immediately follows an earthquake which can reach several millimeters per year, as far as thousands of kilometers away from the epicenter and last for decades or even longer (Khazaradze *et al.*, 2002, Suito and Freymueller, 2009, Trubienko *et al.*, 2013, Klein *et al.*, 2016, Hu *et al.*, 2016). The latter results from the relaxation of stress in the underlying viscous mantle and takes place at the continent scale. Detecting and quantifying such small deformation is a challenge, but sheds light on fundamental properties of the Earth mantle like the viscosity of its different layers (Trubienko *et al.*, 2014). In turn, a more precise quantification of these numbers allows to improve the prediction of long term deformation induced by megathrust earthquakes, glacial-melt isostatic rebound, and relative ground sea-level variations at coastal areas.

We report here on the processing of a large cGPS network deployed by many different institutions across the South American continent over the years. This network has the primary goal of measuring crustal deformation associated with

the physical process of plate tectonics and earthquake cycle. Combining data in Chile with publicly available data from other national and international cGPS networks in South America, we provide a precise and consistent solution spanning 20 years at the continental scale. This solution is provided in the form of a database of time series at ~ 220 selected GPS stations, starting as early as 2000 when possible and currently until the end of 2020. These time series depict precise daily coordinates in the global reference frame ITRF2014 (Altamimi *et al.*, 2017). Many different signals are present in those time series, such as instantaneous jumps attributed to either instrumental changes or earthquakes, and transient deformation attributed to different processes of either tectonic origin (*e.g.*, slow-slip earthquakes) or non-tectonic origin (*e.g.*, seasonal variations of hydrological loads). The precision of the processing is such that it allows the detection and quantification of very small co-seismic offsets (as small as 1 mm) at large distances from moderate size earthquakes (~ Mw 6.5) that frequently occur in Chile. Thus, we provide tables of co-seismic displacements for 55 identified earthquakes. That database will evolve with time, aggregating more data. In the future, we also plan to complement that database with a rapid solution in quasi real time processed in PPP, and with hourly atmospheric delays associated to water vapor content of the lower layer of the atmosphere.

2 Data processing

2.1 Data description

As of today, we only process observations from the GPS constellation, but futures updates of this solution will include observations from other GNSS constellations, and in particular from the European Galileo. We process most of the GNSS data from the national Chilean network (Báez *et al.*, 2018), between 18°S and 40°S, *i.e.*, in the area of Chile where the subduction is rather linear and "simple". North of 18°S, in the Arica bend, the trench curvature induces a rapid change of obliquity and increasing distance of the coastline from the trench. South of 40°S, plate tectonics becomes more complex with partitioning of the oblique convergence along the Liquiñe-Ofqui strike-slip fault (Cembrano *et al.*, 1996). Additionally, towards the South, the continent becomes narrower, making more difficult the definition of a stable plate interior reference frame to study the tectonic deformation. Also, logistics become increasingly difficult at higher latitudes, which renders the cGPS network less dense and more difficult to maintain over a long period of time. Throughout Chile, the national data set is also complemented by local dense networks aiming at studying specific questions in targeted areas (*e.g.* Klein *et al.*, 2021). In addition and in order to realise a continental scale processing, we include data of a selection of stations from the Argentine RAMSAC network (Piñón *et al.*, 2018) and of the Brazil RBMC network. This selection is made in order to reasonably spatially sample the whole continent. We also include all the IGS stations available on the South American continent. This whole data-set is composed of up to 220 stations providing data between 01/01/2000 and currently 31/12/2020.

2.2 Processing strategy

We processed this data-set using the GAMIT/GLOBK software following the classical MIT methodology (Herring *et al.*, 2010a, Herring *et al.*, 2010b). GAMIT uses a so-called double-difference of GPS satellite phase measurements among all pair of sites. Because of the tremendous networks expansion through time, the double-difference approach cannot be applied to the whole data-set in a single network over the whole period. Before 2008, all stations are processed simultaneously in a single network (net CHIL). From 2008 onwards, we divided the processing into 3 sub-networks, based on geographical criteria (Fig. 1). First, we design a continental-scale sub-network, with a total of 75 stations spanning the whole South-America (subnet SAM1). The second group, includes about 70 stations spanning Central Chile and Central Argentina (subnet CHL1). Finally, the third sub-network includes slightly more than 60 stations spanning the northern regions of Chile, Argentina and Brazil (subnet CHL2). Up to 30 stations are common to the 3 sub-networks to ensure a reliable and stable combination of the sub-networks over the years. The numbers of stations in the sub-networks and in total varies quite significantly over time, due to stations showing up late or being decommissioned at some stage. The actual number of stations per day in each subnetworks is represented in Figure 2.

In a first step, we reduce the 30 s sampling data of 24-hour sessions to daily estimates of station positions using the GAMIT software (Herring *et al.*, 2010a), using the ionosphere-free combination, and fixing the phase ambiguities to integer values. Overall, we follow the conventions recommended by IGS in the frame of the third reanalysis of the full history of GPS data collected by the IGS global network since 1994. We use precise orbits from the International GNSS Service for Geodynamics (IGS) (Dow *et al.*, 2009) and IGS tables to describe the phase centers variations of the antennas. We use the Vienna Mapping function (VMF1) derived from numerical weather models for the mapping of the hydrostatic and wet tropospheric delays (Boehm *et al.*, 2006). We estimate one tropospheric vertical delay parameter per station every 2h and 2 spatial gradient parameters on E-W and N-S directions per day. The complete parameters file used in GAMIT is available on the database repository. We also provide our *station.info* file listing all the known equipment changes used in our processing. We update this file over the years, checking and cross-checking metadata made available to us from different local sources (station descriptions, logsheets, rinex headers, field reports, stations visits, ...).

In a second step, daily h-files that include adjusted parameters with their associated variance/covariance matrix for each sub-network are combined into one single continental h-file per day, using GLOBK. Such a solution is called "loosely" constrained, because only relative coordinates are precisely determined. We then use the PYACS toolbox to map the loosely constrained solutions onto the ITRF2014 (Altamimi *et al.*, 2017). This is done by estimating the 7 parameters (3 translations, 3 rotation and a scale factor) of the Helmert transformation between our solution and an up-to-date cumulative IGS reference solution (here *IGS21P01.ssc*). PYACS uses the IGS discontinuity file regularly updated by the IGS analysis combination center (Rebischung, 2021), together

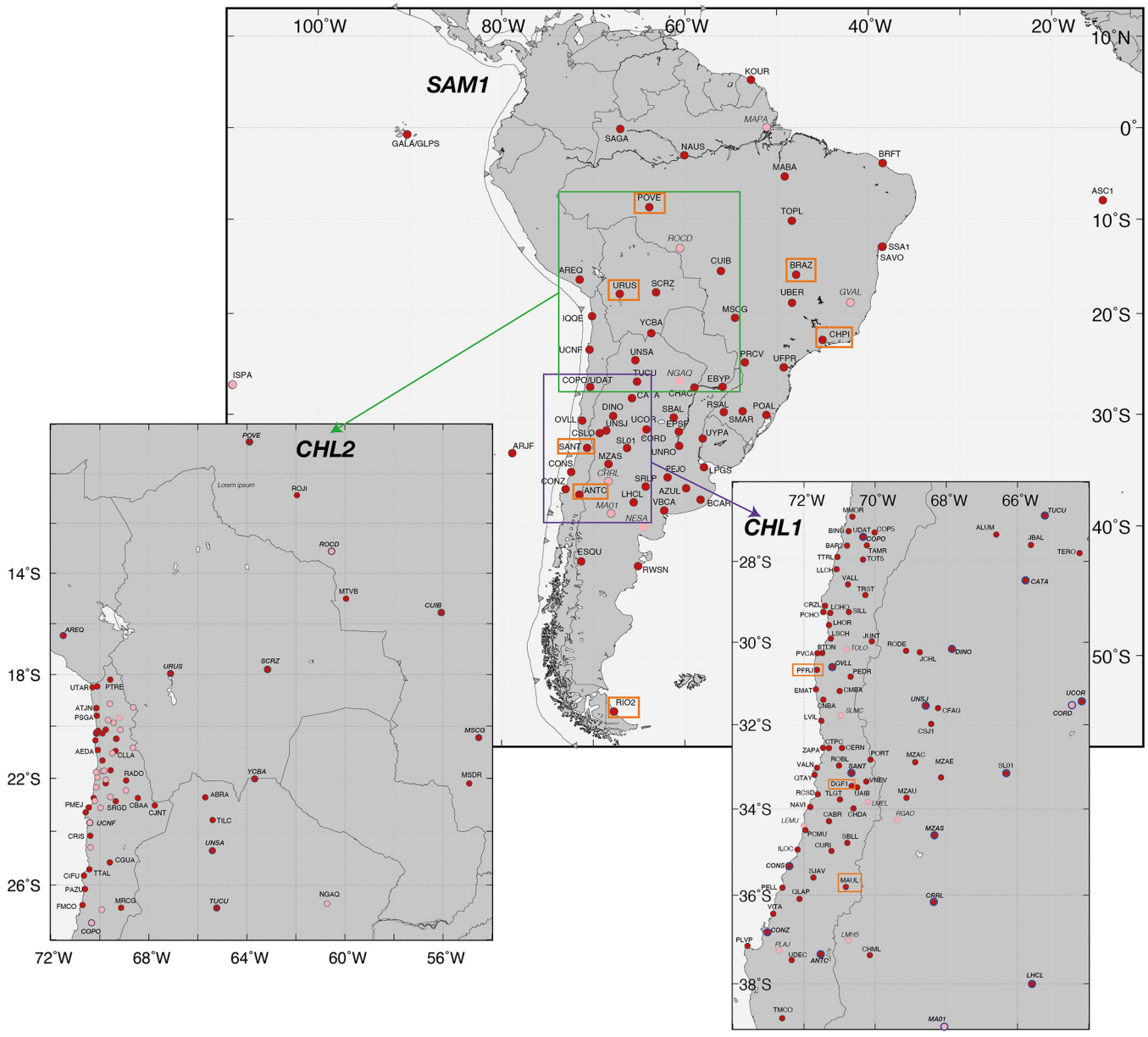


Fig. 1. Maps of the 3 sub-networks used for the GAMIT processing. All stations are not present at every epochs, stations represented in pink did not send data for more than 2 years (either permanently decommissionned or temporary out of commission). On maps of sub-networks CHL1 and CHL2, stations commons to several sub-networks are highlighted by 2 different size circles. The network CHIL used for the processing until 2009 is not represented here. Stations highlighted by the orange frame are the one which time series are presented throughout the article.

with the ITRF/IGS parametric model for IGS sites experiencing non-linear post-seismic deformation. This procedure can be implemented either with PYACS or GLOBK. In theory, both should allow to reach similar results and GAMIT/GLOBK is undoubtedly the most advanced package. However, we choose to use PYACS, rather than GLOBK for several practical reasons. First, Helmert parameter estimation is performed by minimizing a L1 norm on coordinates in the topocentric local frame. This approach allows to separate the horizontal from the vertical component and is particularly efficient in identifying the frequent outliers in the vertical component. PYACS also provides a fast mode by neglecting the full variance/covariance matrices for rapid solutions. This mode eventually provides equivalent coordinates precision. This approach, in addition to the choice of using continental stations rather than the full global combination, results in considerable time saving, considering our current computing facilities.

We provide, in the Supplementary Material of this article and on the database repository, a complete list of processed

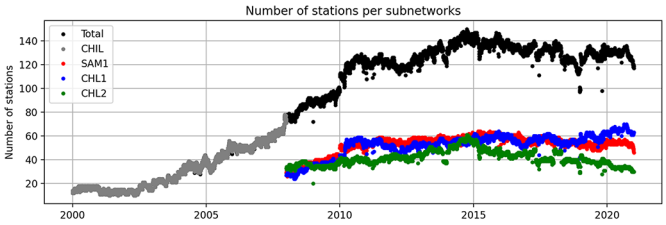


Fig. 2. Number of stations as function of time for the 3 sub-networks. Note that, after 2008, the total curve is not simply the sum of the 3 sub-networks because of common stations.

stations, along with their geographic and Cartesian coordinates and their period of record.

3 Quality of our solution and comparison with existing solutions

3.1 Quality of the solution

Starting with the stabilization part performed using the PYACS software, we note that because of the network density evolution with time, the amount of reference stations also evolves with time, increasing from 10 to 25 over the first decade and eventually stabilizing to 30 during the second decade (Fig. 3). Figure 4 shows the stabilisation network. It is to note that, using such a network aperture, part of the real signal associated to hydrological continental loading (the largest being the Amazonian Basin), can be absorbed in the scale parameter of the Helmert transformation. But only part of it (and hopefully small), since this large scale deformation is affected by gradients that allow to partly separate its contribution from reference frame rotation, translation and scale factor (Fu *et al.*, 2013, Chanard *et al.*, 2018). In any case, such a stabilisation is optimal for the analysis of tectonic signal of the plate boundary, which is our primary concern, as well as the analysis of local sources of any kind (tectonic, hydrological, etc. See examples of deformation processes in section 4) but is probably less appropriate for the analysis of continental scale loading. We show in Figure 5 residuals time series after stabilisation at 3 selected IGS sites, highlighting the epoch used (in red) and the rejected one (in gray) during the Helmert estimation. Stations that show a transient deformation due to the post-seismic processes can still be used as stabilisation stations, because these processes are accounted for in the prediction of the station position in the ITRF2014. For example, at Antuco, at the foothill of the Andes (station ANTC), clearly affected by an intense post-seismic transient deformation, the residuals between the predicted station position and the measured station position are of the order of several millimeters only (Fig. 5A). On the other hand, the case of station URUS in Bolivia highlights the handling of discrepancies between *a priori* and actual velocities by Pyacs (Fig. 5C). That station was only integrated in the ITRF at the end of 2013 and anterior *a priori* coordinates are extrapolated. The definition of the ITRF is therefore not to blame. The important aspect that we want to underline here, is that PYACS automatically and efficiently rejects the station from the stabilisation process before 2014, because there is some inconsistency between ITRF2014 *a priori* values and actual observations, and re-integrates it after 2014 when ITRF2014 *a priori* values and actual observations are in agreement. The tipping date of 2014 corresponds to the occurrence of the 2014 Iquique earthquake, for which new coordinates (position and velocity) were derived after the earthquake. Indeed, although the station has a relatively small co-seismic offset, it exhibits a large change of velocity between before and after the earthquake, especially on the North component (*cf.* section 4.1.1).

We show in Figure 3 the evolution of the number of sites used to compute the Helmert parameters together with the time series of median and the weighted-root-mean-square (WRMS) of residuals (final coordinates minus IGS). Over the 20 years processed, we obtain a quite constant L2-norm postfit WRMS, averaging to less than 1.5 mm in both planimetric components, although variations appears quite larger over the first 3–5 years (Figs. 3B and 3C). Unsurprisingly, the average of L2-norm postfit WRMS on the vertical component is higher, reaching 5 mm, there again with significantly larger variations over the first 3–5 years. Note that we find in the postfit WRMS the seasonal variations that are not taken into account in the current parameterization of the ITRF2014. They become even more visible as the precision gets better with time. We expect to obtain even much flatter postfit WRMS curves when these seasonal oscillations will be accounted for in the ITRF, expected with the next release ITRF2020. However, the mean WRMS are already very small, less than 1.5 mm on both horizontal components for both the L1-norm and the L2-norm.

The daily scatter, defined here as the median of the differentiated time series, is a good indicator of the high frequency noise level of a time series. It is not affected by transient signals such as postseismic deformation. We can therefore compute it on all time series and over the complete period of record. Daily scatter as function of latitude for the 3 components, highlight a geographical pattern (Fig. 6). It appears significantly smaller for stations located between 18°S and 50°S, with sub-millimetric values for the horizontal components and less than 3 mm on the vertical. It is larger for stations located north of 18°S plus south of 40°S (with median slightly larger than 1 mm on the horizontal components and almost 5 mm on the vertical). This seems directly correlated with the density of stations. A lower density implies longer and scarcer baselines, inherently less precise because phase-ambiguity resolution becomes more difficult as baseline length increases. Recent study also showed that non-tidal atmospheric and oceanic loading deformations affect the stochastic properties of vertical motions in a latitude-depend way, which could explain part of the larger daily scatter observed at the extremes latitude of our network (Gobron *et al.*, 2021). In any case, this analysis of daily scatter suggests that we can actually extract sub-millimetric short-term signals from horizontal time-series, like for instance tiny co-seismic offsets.

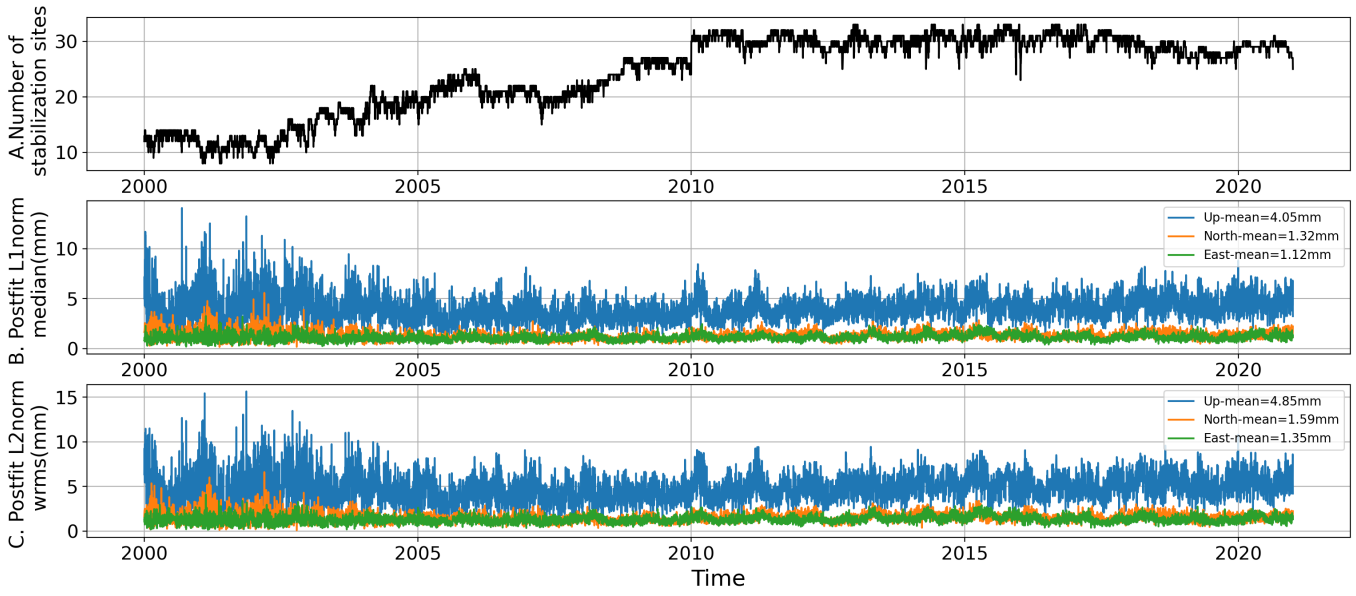


Fig. 3. Evolution of the stabilisation network. (A) Number of reference stations used in the PYACS stabilization as function of time; (B) Daily PYACS postfit L1-norm median (in mm) on the 3 components; C) Daily PYACS postfit L2-norm wrms (in mm) on the 3 components.

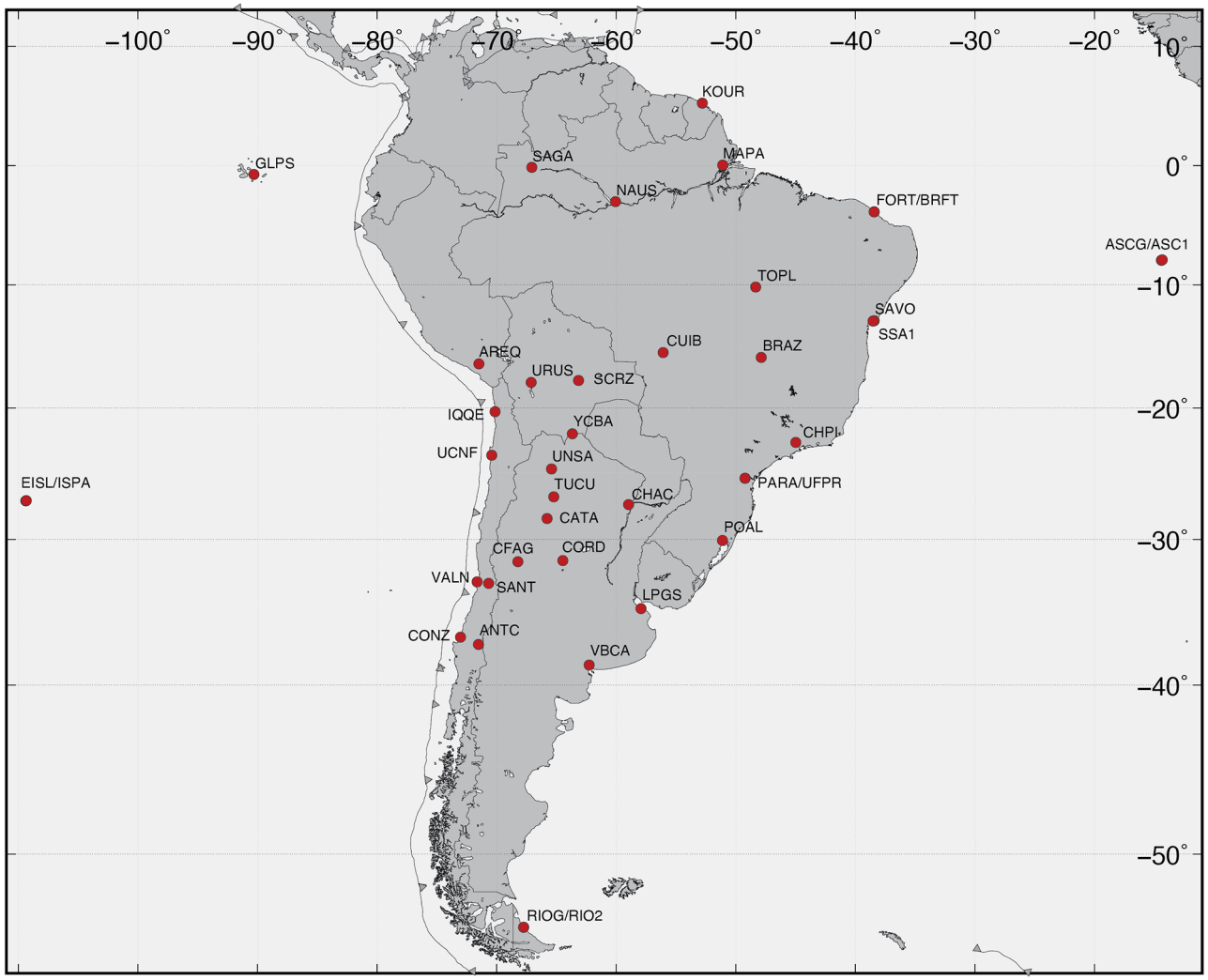


Fig. 4. Map of stations used in the stabilisation process.

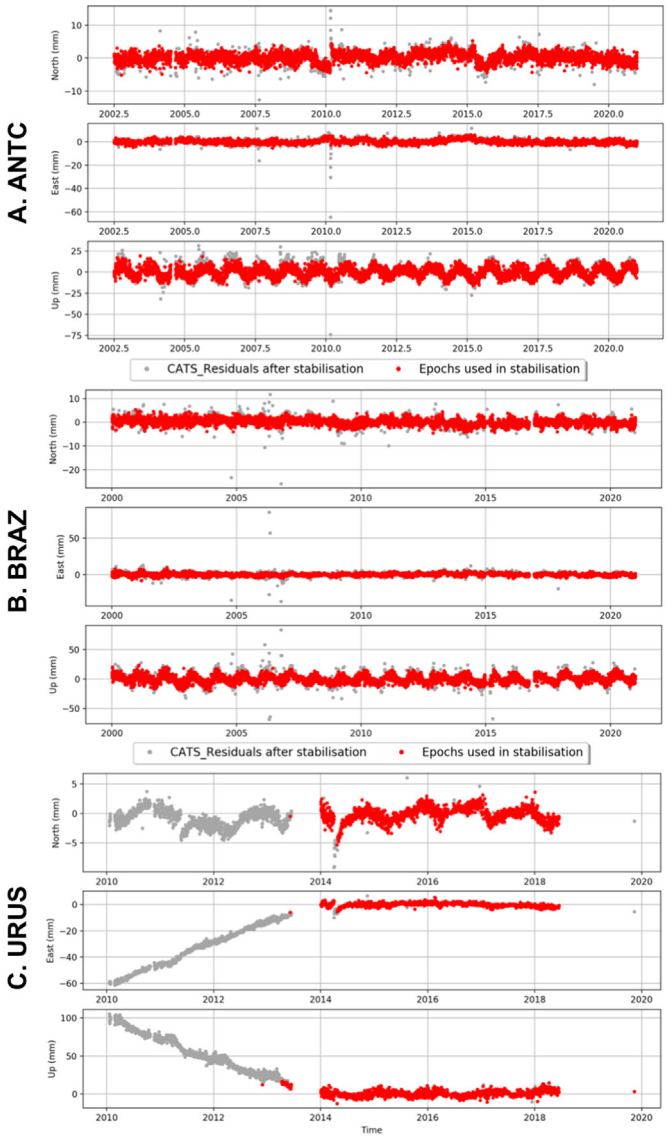


Fig. 5. Residuals time series after stabilisation. For 3 stations: (A) ANTC (in Chile), (B) BRAZ (in Brazil) and (C) URUS (in Bolivia), epochs used in the stabilisation are represented in red, rejected epochs are represented in gray. Location of stations are depicted in Figure 1.

3.2 Comparison with existing solutions

We compare our solution with two existing ones: i) the third IGS reprocessing campaign forming the IGS contribution to forthcoming ITRF2020, Repro3 (Rebischung *et al.*, 2019), ii) the Nevada Geodetic Laboratory solution (NGL, Blewitt *et al.*, 2018). Both Repro3 and NGL solutions are global ones. But these solutions differ on several aspects. Repro3 is a combination of solutions from 10 different Analysis Center (ACs, which are COD, ESA, GFZ, GRG, JPL, MIT, NGS, TUG, ULR, WHU). This combination therefore includes solutions that differ regarding the included constellations (some ACs process only GPS, other include GLONASS and/or Galileo). The NGL solution uses a PPP approach including more than 15 000 stations globally available.

Here, we compare time series of specific interest from a selection of stations across the whole continent: SANT (near Santiago de Chile) is an IGS station located near the central part of the Chilean subduction zone (Fig. 7-I.A), CHPI (between Sao Paolo and Rio de Janeiro) is an RBMC-IGS station located on the so-called Brazilian craton (Fig. 7-II.A), and RIO2 (in Patagonia) is a RAMSAC-IGS station located at the extreme south of the continent (Fig. 7-III.A). All 3 have long lasting and complete times series and contribute to our stabilization network. The 3 time series are simply detrended but otherwise unfiltered. SANT is showed only between 2000 and 2010, period over which its motion is linear with time and unaffected by any large earthquake. CHPI and RIO2 are showed over the time period over which the 3 solutions provide a coordinate. Our solution is overall smoother, with a lower level of high frequency noise. It also depicts smaller WRMS on the 3 components and in particular on the vertical component. This WRMS reduction comes from low frequency noise reduction, rather than from the reduction of the high frequency noise, since the latter is only a small contribution to the overall series variance (see Fig. 7B). It has been showed that regional GPS solutions show lower noise than global solutions, which is the case of the NGL and IGS solutions (Williams *et al.*, 2004). Therefore, part of the noise reduction described by our solution can result from continental stabilisation, which aperture remains significantly larger than expected from a regional solution. At SANT, low frequency "oscillations" are observed (Fig. 7-I.A). However, their amplitude are significantly lesser in our solution. Therefore, they are most likely to be coming from the stabilization process. Most of the reference frame oscillation, which appears as continental scale common mode noise, is absorbed by the continental stabilisation made with PYACS. RIO2 is an exception on which we observe strong oscillations on the north component of our solution (Fig. 7-III.A). We also observe, on all 3 solutions, offsets in 2012 and a following change of trend until 2020 when equipment was changed again. The 3 solutions disagree on the amplitude of the documented instrumental changes, which comes from how it is handled in the processing (for ex. the weight applied on observations or the quality of the wet troposphere corrections).

For these 3 stations, we compute the Lomb-Scargle Power Spectral Density (Fig. 7B) of the 3 detrended components. All spectrum show similar pattern with white noise dominating at high frequency corresponding to periods of a few days to weeks, and power increasing with lower frequency attesting for colored noise (Williams *et al.*, 2004).

In the details, the north component of SANT time series shows an interesting behaviour (Fig. 7-IA): Recurrent small incremental southward motion (*i.e.*, in 2003.5, 2004.5, 2005.5). These signals are visible on the 3 solutions but with different characteristics. On the NGL solution, which has a significantly larger daily scatter, they show as ramps, which can be approximated by a sinusoidal function and may be partly absorbed by a seasonal filter. In our own solution, with lesser daily scatter, they show as offsets. On the Repro3 solution, with intermediate daily scatter, they show as a mixture of ramps and offsets. Finally, on our solution with the

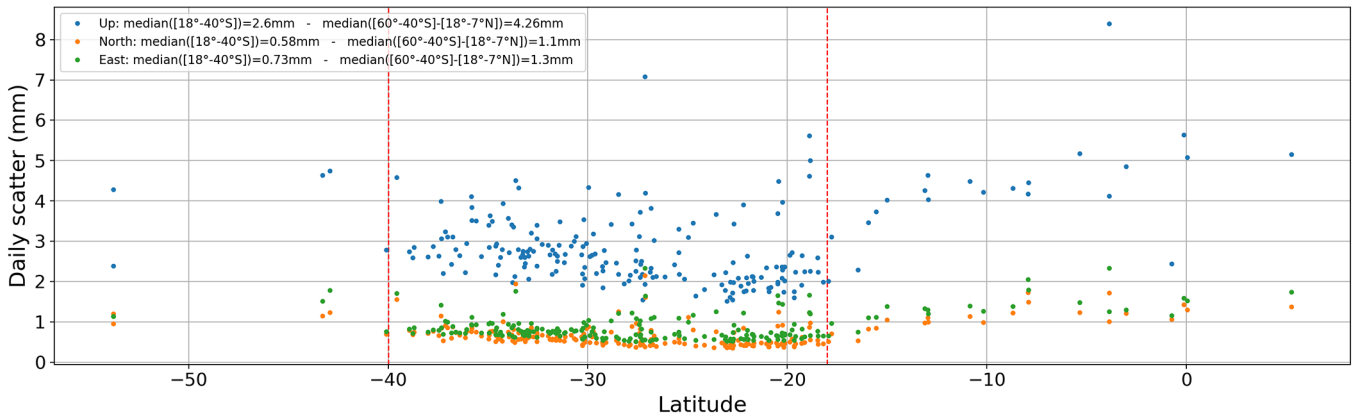


Fig. 6. Daily scatter as function of latitude (in mm) on the 3 geographic components of station coordinates (Up-blue, North-orange, East-green). Median values of daily scatter estimated on the 3 components for 2 groups of stations are showed in the upper left inset: (a) between 18°S and 40°S where there are many, (b) south of 40°S plus north of 18°S where there are scarcer.

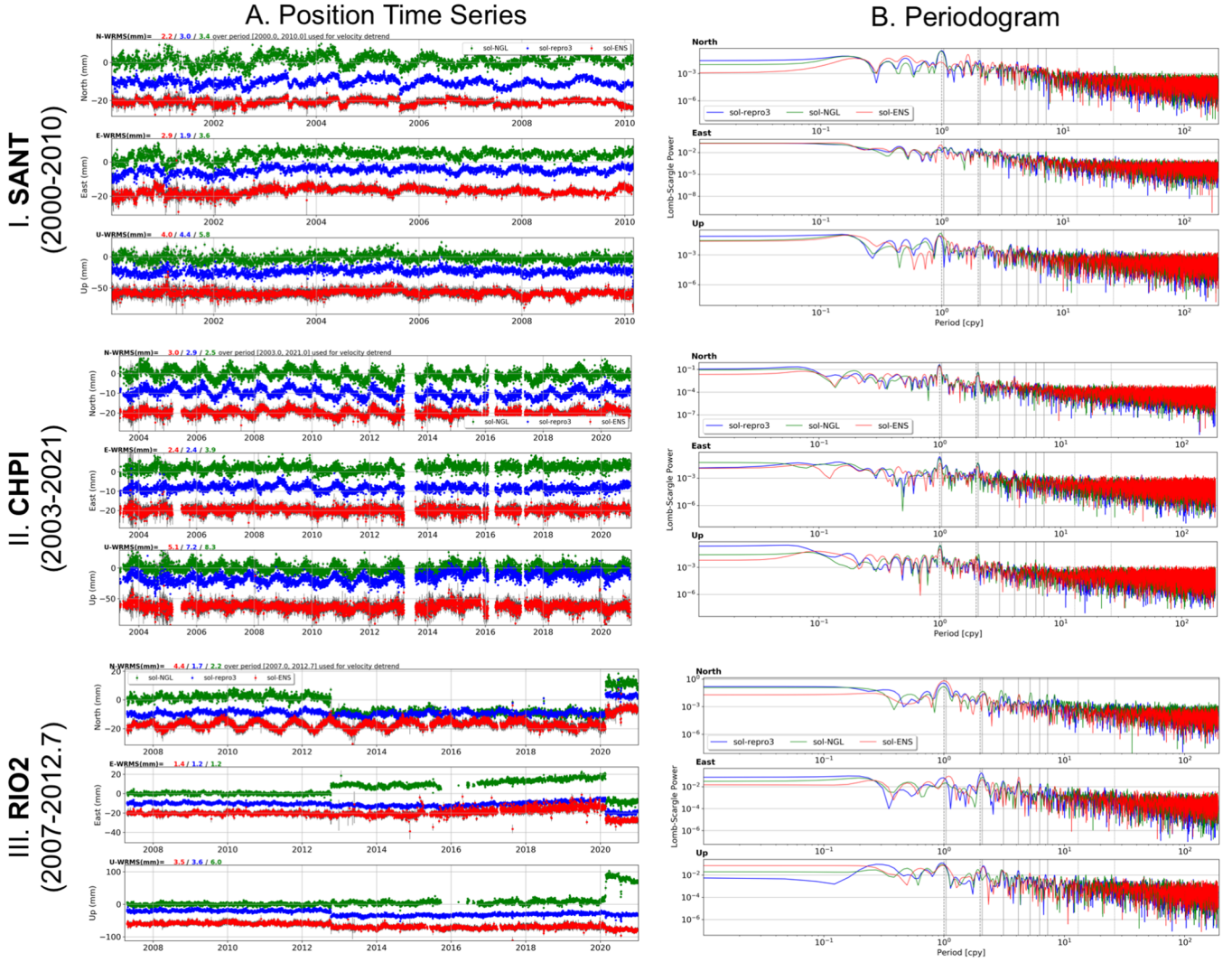


Fig. 7. Comparison of 3 different GNSS solutions at 3 sites: SANT, CHPI and RIO2. (A) (left panel) detrended North-East-Up components of position time series of NGL (green dots), Repro3 (blue dots) and our solution (red dots). (B) (right panel) Lomb-Scargle periodograms of the 3 solutions at the same 3 sites. For each stations, the same period is used to estimate the trend and compute the WMRS and periodogram (SANT:2000–2010; CHPI:2003–2021, BRAZ:2007–2012). Stations locations are depicted in Figure 1.

smaller daily scatter, some structures start to emerge when they are drowned in the higher noise of the other solutions. This is discussed further in section 4.3.

One of the advantage of a post-processed solution is to ensure, through frequent databases synchronisation and reprocessing, that time series are complete over time. In some regions, this is a critical aspect. For example, most stations located in the region of the Illapel earthquake of 2015 in Chile, show a 2–3 years data gap in the NGL process between ~ 2010 and 2013 (*cf.* example of station CNBA, Fig. S1, in Supplementary Material). This gap has been pointed out in recent articles (*e.g.*, Yuzariyadi and Heki, 2021), but is only a processing gap, not a data gap since these stations were operational and their data collected, but possibly not available to NGL at the time of their processing. Such large gaps can challenge the interpretation of observed signals. For example, a vertical offset shows up during this time window at all these stations in the NGL solution. These offsets can be interpreted as coseismic offsets, or anything else happening to the stations during this time frame, but are actually not real since they do not appear on any of our time series.

4 Examples of deformation processes

In the following, we qualitatively describe several examples of the signals that are present in our time series and that shed light on the different types of studies that can be performed using them. In addition, we also point out a few signals that still need further investigation to be fully understood.

4.1 Seismo-tectonic processes

4.1.1 Surface deformation associated with the seismic cycle along the Chilean subduction zone

Because of the occurrence of 3 major earthquakes along the subduction zone (Mw 8.8 in 2010, Mw 8.1 in 2014 and Mw 8.3 in 2015), several years after the beginning of the deployment of cGPS networks in Chile (end of the 90's), the 3 phases of the seismic cycle (pre-, co- and post-) could be observed in great details. To illustrate what is actually observed, we show stations affected by the 2010 Maule earthquake (ANTC & MAUL, Fig. 8A), the 2014 Iquique earthquake (URUS, Fig. 8B) and the 2015 Illapel earthquake (PFRJ, Fig. 8C).

Convergence of the Nazca plate towards the South American plate results in deformation along the Chilean margin induced by locking at portions of the subduction interface. This slow and continuous deformation can last centuries. This is the interseismic phase, of which we observed only the last decade or so, and which appears as a linear trend before 2010 at MAUL and ANTC, and before 2014 at URUS. When enough deformation has accumulated, an earthquake occurs, which generates a deformation of the surface in only a few seconds to minutes. In daily time series, these coseismic offsets show as instantaneous jumps between the positions of the days before and after the earthquake. Depending on whether the earthquake occur early or late in the day may shift the jump from the difference between the day before and the day of the earthquake to the day of the earthquake and the day after. Following the largest earthquakes (Mw larger than 7), a significant transient deformation, called post-seismic deformation, occurs and can be observed. Often approximated by a logarithmic or exponential functions, this deformation can last for decades but decreases with time (see for ex. the 1960 Mw 9.5 Valdivia earthquake, Barrientos *et al.*, [1992]). Because of the geometry of the Chilean subduction striking North-South and the almost East-West motion of the Nazca plate relative to South America, most of the surface deformation is usually observed on the East component of GNSS time series. This is what we observe at ANTC and MAUL in February 2010, where the westward coseismic offset reached close to 1 m against only about 20 cm on the North-South component. The post-seismic deformation observed at these stations also follow that rule (see a detailled analysis of the postseismic deformation following the Maule earthquake in Klein *et al.* [2016]).

Station URUS, located at about 200 km in the North-East of the epicenter of the 2014 Iquique earthquake is particularly interesting because it does not follow that rule (Fig. 8B). The coseismic offset on the East component is about twice as large as the one on the North component (1.6 cm westward *vs.* a 0.8 cm southward, see table 2014-04-01.dat from the coseismic data base hereafter described). However, four years after the earthquake, the trend on the East-West component is almost back to the pre-earthquake trend. This is not the case on the North-South component, where the postseismic trend still remains very different and has not returned yet to the pre-seismic trend. This is due to the different geometry: the location of the station with respect to the earthquake, as far north as east from the epicenter.

Station PFRJ, located very close to the 2015 Illapel earthquake epicenter shows more complexity (Fig. 8C). As expected, the co-seismic displacement is dominated by the East-West component. However, the lesser displacement of the North-South component reveals that if the co-seismic jump is southward, the post-seismic deformation that follows is northward, and affected by short term transients. A similar observation can be made on the vertical component: the co-seismic displacement is downward, but the displacement that follows is upward and rapidly changing with time. These post-seismic displacements reveal a combination of jumps due to aftershocks and rapid sliding due to after-slip on the subduction interface. Both phenomenons occur on the subduction interface, which is close to the coastline where the station is located.

4.1.2 Catalog of coseismic deformation due to the major Chilean earthquakes

Having a coherent reanalysis of 20 years time series, we built a data base of coseismic offsets estimated for all events of Mw larger than 6.5 that occurred over the period along the Chilean subduction zone. We found 55 earthquakes on the USGS catalog, that are represented in Figure 9 with their focal mechanisms extracted from Global CMT (Dziewonski *et al.*, 1981, Ekstrom *et al.*, 2012). About a third of the events belongs to aftershock sequence of one of the 3 megathrust earthquakes of magnitude above 8: 2010 (Maule), 2014 (Iquique) and 2015 (Illapel). For events that are occurring on the same day (for ex. a Mw 6.8 and a Mw 6.5 occurred on 1 September 2020 in the Atacama region) or on two consecutive days (for ex. a Mw 7.7

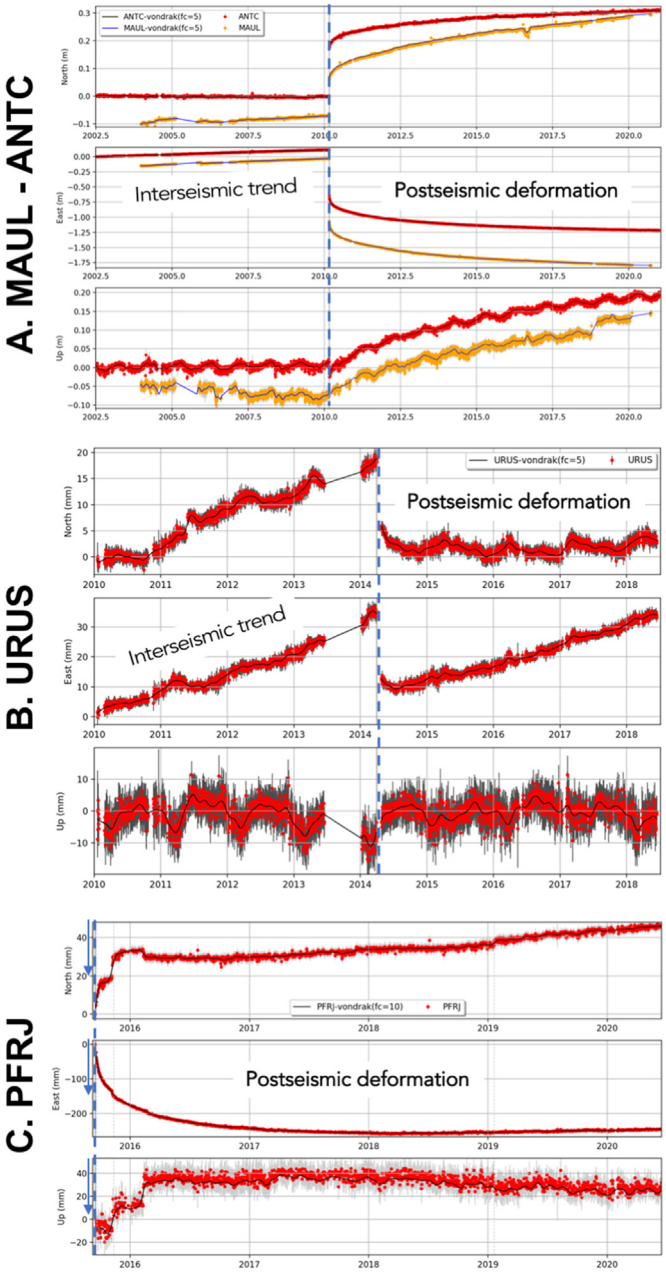


Fig. 8. Surface deformation associated with seismic cycle. North-East-Up components of time series from our processing at different stations: (A) ANTC (red) and MAUL (orange), in Chile, located at the foothill of the Andes in the region affected by the 2010 Maule earthquake; (B) URUS in Bolivia, in far field of the 2014 Iquique earthquake; (C) PFRJ in Chile, located on the coastline in near field of the 2015 Illapel earthquake. For (C), since we show only the postseismic period, the blue arrows depict the direction of the coseismic displacements. All time series are represented relative to stable South America. All time series are highlighted by Vondrak filters, which cutoff frequencies in cycle per year are indicated in figures insets (dark full lines). Location of stations are depicted in Figure 1.

occurred on 14 November 2007, the Tocopilla earthquake, its largest aftershock of Mw 6.8 occurred on the following day, Fig. 9-inset), we estimated cumulative coseismic offsets induced by both events. Eventually, this leaves a list of only 44 events.

In order to provide an homogeneous data base, we applied an automatic approach identical for all events. We use the raw time series without correcting for outliers or trends nor applying any filtering. A detailed description of our algorithm can be found in the Supplementary Material. Eventually, 36 events trigger a non-Null offset at at least one station (*cf.* Table in the Supplementary Material). For each of these 36 events, we provide an ASCII table (and a regional map of the coseismic offsets (for ex. Fig. 9-inset). All tables include a comprehensive header detailing its content (*cf.* Supplementary Material). All figures and tables are available on the ftp deposit.

Considering the methodology applied, care should be taken when considering one particular event. Our goal here is to provide a database that is homogeneous and includes small earthquakes at the limit of detectability of the network. The fact that coseismic displacements corresponding to these small earthquakes are detectable in the time series of several stations is often ignored. However, the quantification of a very small offset is often difficult and some tuning of the algorithm would be required depending on the specific conditions of the affected stations (data gaps, noise level, presence of simultaneous transients, etc.). Therefore, when interested in a particular event, it is best to re-evaluate the offsets, using a more thorough and adaptive methodology on filtered time series. For that same reason, the coseismic tables extracted here for the 3 megathrust earthquakes can hardly be compared with previously published tables (such as, Vigny *et al.*, 2011, Ruiz *et al.*, 2014, Klein *et al.*, 2017) for which additional filtering and corrections, including removal of after-slip, were applied.

4.2 Seasonal deformation

GPS time series are notoriously affected by seasonal oscillations. Typically, these seasonal oscillations are often described by annual and semi-annual terms and thus removed by fitting a pair of sinusoidal terms to each time series (Nikolaidis, 2002). Although powerful, this method has some drawbacks. First, seasonal signals do not necessarily have constant amplitude nor phase cycles, they can be shifted in time (either because the meteorology itself is delayed, or because of delays in the Earth response to a changing seasonal load). Thus, the fit by a pair of sinusoidal terms of constant phase and amplitude is not perfect and can leave a significant misfit. Worse, it can introduce a bias (through aliasing) on the long term trend determination.

Despite the fact that most of Northern-Chile is a desert, there is a seasonal cycle visible in GPS data in this area. This cycle certainly originates from the hydrological load of the Amazonian basin and possibly from local atmospheric loading. The Amazonian basin hydrological load is huge: a vertical

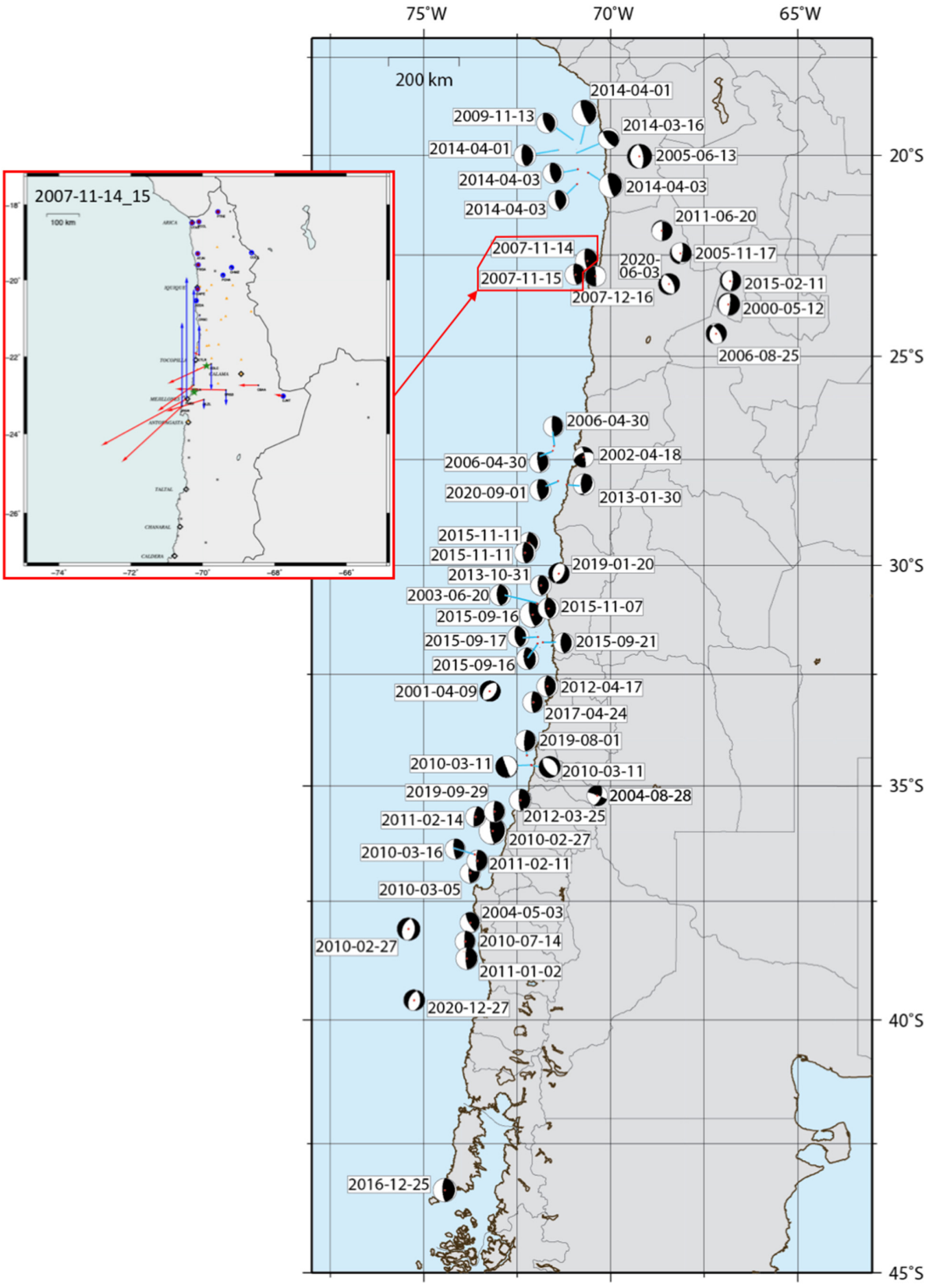


Fig. 9. Map of the 55 earthquakes of Mw 6.5 and larger included in the coseismic offsets data base. Epicenters are from USGS, and focal mechanisms from global CMT. The inset shows the combined coseismic field estimated for the Mw 7.7 and 6.8 earthquakes that occurred on 14th and 15th November 2007 in North Chile (The Tocopilla earthquake and its largest aftershock). See Supplementary Material for examples of a complete table and times series.

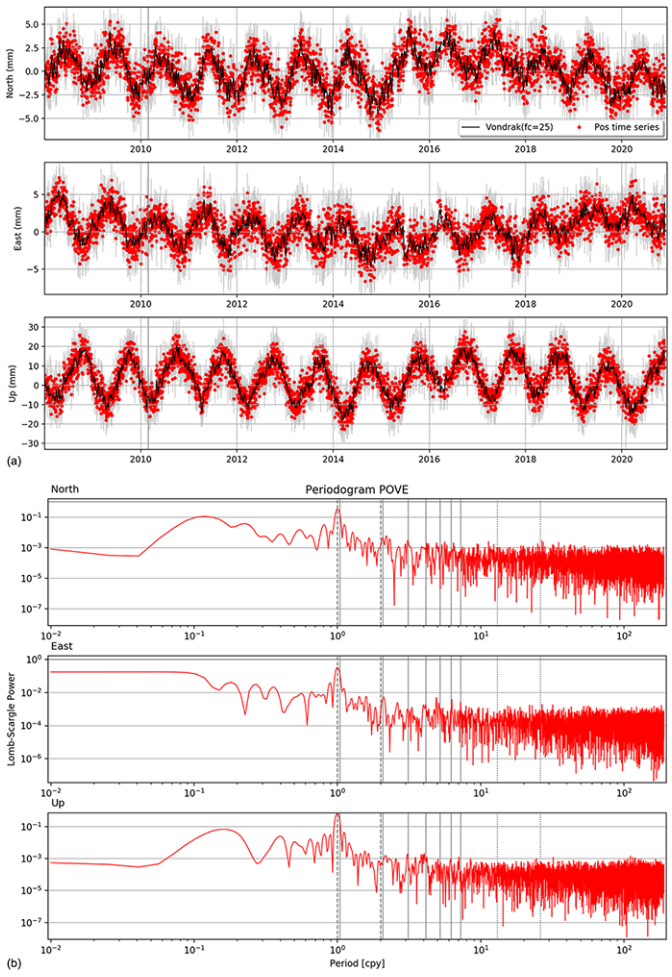


Fig. 10. Seasonal deformation at station POVE. (a) North-East-Up components time series from our processing, detrended after outlier elimination. The time series are highlighted by a Vondrak filter of cutoff frequency 25 cpy (black line). (b) Lomb-scargle periodogram of the detrended and cleaned time series over the displayed period of observation. Expected periods are represented by the vertical line (gray dashed: annual and semi-annual period; gray solid: draconitic period and harmonics; dotted line: fortnightly tidal cycle and harmonic of ~ 14 and ~ 28 days). Location of POVE is depicted in Figure 1.

cycle of up to 4 cm and an horizontal cycle of up to 1 cm peak-to-peak is clearly observed at PortoVelho (POVE, Fig. 10a) which is located in a meander of river Rio Madeira, the biggest tributary of the Amazon, no more than 1500 km North-East of Iquique in North Chile. It is a very long wavelength signal, so stations in a given area of Chile will have almost the same cycle and most of this signal will cancel out when differenciating. However, small but significant differences of several millimetres (both in horizontal and vertical components) can be observed at stations several hundreds of km apart (*e.g.*, Fu *et al.*, 2013, Chanard *et al.*, 2018). Finally, the periodogram of POVE (Fig. 10b) reveals a richer frequency content than the simple annual/semi-annual standard estimation. We do not detect any other clear period, such as the draconitic period (351.6 days), which cannot be separated from the annual solar period with less than 26 years of data. However, it reveals that the 6-month peak amplitude is in reality much smaller (two order of magnitude, on the 3 components) than the 12-month peak. This is very different from the classical simple estimation of only an annual and semi-annual terms, which usually finds the two terms to be of comparable amplitude. This finding suggests that the amplitude of this semi-annual term can be significantly but artificially inflated through aliasing with nearby frequencies when estimated alone. Some periodograms indeed show several pics around but not exactly at 6 months (Fig. 7B).

4.3 Transient deformation

GPS time series also reveal a lot of transient signals, lasting between several days to several years, potentially repeating with more or less regular periods. Transient deformation can be generated by a whole range of different sources such as volcanic deformation, oceanic or atmospheric loading effects, and again hydrological loads, depending on the ground composition and/or seasonal and multiyear groundwater variations (*e.g.*, Silverii *et al.*, 2016).

However, many transients observed in subduction zones are associated with faulting processes, such as postseismic deformation (following major earthquakes, explained in section 4.1.1) or Slow Slip Event. These can have variable duration and potentially be recurrent, as in the region of Copiapo (Klein *et al.*, 2018). In some cases, they can precede earthquakes and contribute to the initiation of the main shock rupture, as for the 2014 Iquique earthquake (Ruiz *et al.*, 2014, Socquet *et al.*, 2017, Boudin *et al.*, 2021) or the 2017 Valparaiso earthquakes (Ruiz *et al.*, 2017).

Some observed transient signal remain hard to relate to any known sources. As an example, we show the time series of SANT and DGF1, both in the Santiago de Chile metropolitan area, separated by about ~ 35 km (Fig. 11). SANT time series exhibits regular events on the North component (previously mentioned section 3.2), characterized by a transient northward sliding, interrupted by a sudden southward jump, followed by the resumption of the northward sliding (for ex. mid 2003, mid 2004 and mid 2005). The station DGF1 was only installed in 2004, but rapidly exhibits a northward transient simultaneously with SANT. Santiago is located in a sedimentary basin, which is plausibly affected by hydrological processes which could have variable impact depending on the location and the monumentation of the stations (outcrop or building rooftop, depth of anchoring, etc.).

Such transient signals of currently unknown origin are difficult to deal with, because they are small and show differently on different solutions: jumps and offsets in our solution, continuous ramps of changing slope in NGL solution (Fig. 7-I). Because it has a low daily scatter, our solution appears appropriate to extract the details of these kind of events, but extra-care should be taken to avoid over-interpret signal that could be related to the monumentation of the stations or, in some extent, to the data processing. Typically, a careful consideration of offsets and different noise types is necessary for a correct modeling of time series, which is most of the time very challenging.

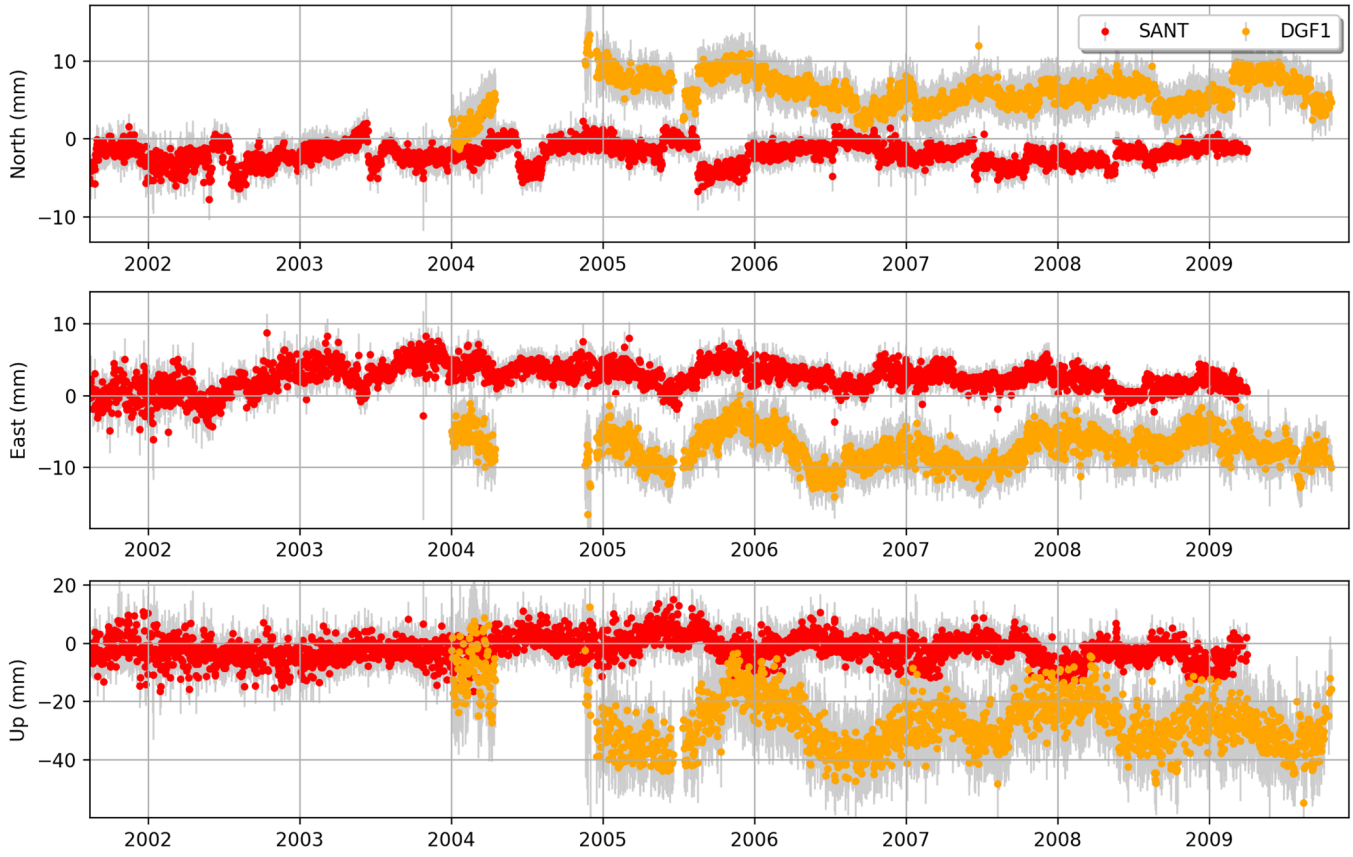


Fig. 11. Example transient deformation. North-East-Up components of detrended time series at SANT (red) and DGF1 (orange) from our processing. Location of stations are depicted in Figure 1.

5 Diffusion of products

All products (time series, coseismic tables) can be downloaded on a ftp deposit (ftp://ftp.geologie.ens.fr/incoming/tempo/SOAM_GNSS_solENS/). They are all named *SOAM_GNSS_solENS*, followed by the type of product (currently *_Pos* or *_Coseismic*) and the release version. The present solution is the release v1.0 and will evolve with time: a reprocessing due to parameter changes will be reported by an increase of the first index (for ex. v2.0), the addition of new data will be reported by an increase of the second index (v1.1). For coseismic offset tables (and all future products), the release version refers to the GNSS solution used. Station's time series come as *pos file*, a standard format, explained in detail in the file header. We knowingly choose to disseminate raw time series, ie unfiltered and unmodeled, in order to allow users of any community (seismotectonics, atmosphere, hydrology, . . .), to use them without any misconception about the data content or filtering.

6 Evolution of the data base

Our data base is meant to evolve with time. First, and as previously explained, the current solution will evolve, including more recent data (a solution up to the end of 2021 will be made available early 2022), or integrating new processing parameters. The coseismic offset data base shall be updated simultaneously. Second, we also plan to propose more products, first with a solution processed in quasi real time following a PPP strategy (Zumberge *et al.*, 1997). This solution will be significantly less complete since some data are arriving with up to several months of delay. But it would allow the release of a very quick partial solution, for example after future major earthquakes. Similar quick solutions could be provided for high rate GNSS as well, at least at all stations where 1 Hz data are acquired.

We also plan to provide hourly atmospheric zenithal delays at every station. Tropospheric zenithal delay time series can be used as a proxy of the water vapor contained in the troposphere above the stations and be used in meteorology.

Finally, the diffusion channel of our products will evolve. We are currently developing a web application, composed of i) a web mapping showing the processed network and allowing to access to stations metadata, ii) a web application that will allow to visualize, manipulate and analyse position time series, based on the Pyacs suite. ASCII files of time series will therefore be downloadable through both pages, raw or analysed.

Conclusions

For more than 20 years, our research group has been using GNSS data to work on the Chilean subduction. To do so, a long

and thorough work of processing of the data produced by more than 200 stations located across the whole South-American continent has been led over time. Today, and after a complete and thorough reprocessing of data acquired between 2000 and 2020, we aim at sharing that consequent database with all research communities interested by GNSS data in South-America. Even though we are not an observatory and neither mandated nor funded to do so, we will do our best effort to maintain, upgrade and share this solution.

Supplementary material

Figures S1 to S5.
Section S1 detailing the coseismic offsets estimation.
Table of the 55 earthquakes composing the coseismic offset data base.
The complete list of processed stations with their coordinates and period of record.

The Supplementary Material is available at http://www.bsgf.fr/10.1051/bsgf/2022005/olm.

Acknowledgments. We would like to warmly thank the numerous people who have, over the years, installed and maintained the stations, and also made possible the free access to data and metadata. This work, and any of the great scientific contributions based on these GNSS data, could not have been done without their collective work. This includes (but not only), all the CSN staff, in particular J.C. Baez, all the RAMSAC staff, in particular Demian Gomez and Diego Piñón and all the RBMC staff. These acknowledgements are also directed to all the French and Chilean participants who contributed to the beginning of permanent GNSS development in Chile among whom (but not limited to, in alphabetical order) Carlos Aranda, Carolina Bermejo, Sylvain Bonvalot, Jaime Campos, Daniel Carrizo, Jean-Bernard de Chabalier, Germinal Gabalda, Raúl Madariaga, Sylvain Morvan, Manuel Olcay, Ismaël Ortega, Alain Rudloff, Jean-Claude Ruegg, Anne Socquet, as well the Caltech and OSU north-American teams, and the German GFZ teams. The authors also want to sincerely thank Mike Floyd for his very precious and constant help regarding the GAMIT/GLOBK process, as well as the whole MIT team developing the software. We also want to thank Paul Rebischung for facilitating access to the Repro3 solution and J. B. Besnier, T. Jezequel, T. Mesure and C. Peutin for their significant contribution in the development of the web applications. Finally, we sincerely thank our two reviewers Nicola D'Agostino and Alvaro Santamaria-Gomez for their very constructive reviews.
Maps are made with Generic Mapping Tools GMT (Wessel *et al.*, 2013). Python tool-boxes used: PYACS+ PYEQ (https://github.com/JMNocquet/pyacs36), ASTROPY.

References

Altamimi Z, Collilieux X, Legrand J, Garayt B, Boucher C. 2007. Itrf2005: A new release of the international terrestrial reference frame based on time series of station positions and earth orientation parameters. *Journal of Geophysical Research: Solid Earth* 112 (B9).

Altamimi Z, Métivier L, Rebischung P, Rouby H, Collilieux X. 2017. Itrf2014 plate motion model. *Geophysical Journal International* 209(3): 1906–1912.

Angermann D, Klotz J, Reigber C. 1999. Space-geodetic estimation of the Nazca-South America euler vector. *Earth and Planetary Science Letters* 171(3): 329–334.

Báez J, Leyton F, Troncoso C, del Campo F, Bevis M, Vigny C, *et al.* 2018. The Chilean GNSS network: Current status and progress toward early warning applications. *Seismological Research Letters*.

Barrientos SE, Plafker G, Lorca E. 1992. Postseismic coastal uplift in southern Chile. *Geophysical Research Letters* 19(7): 701–704.

Beck S, Barrientos S, Kausel E, Reyes M. 1998. Source characteristics of historic earthquakes along the central Chile subduction zone. *Journal of South American Earth Sciences* 11: 115–129.

Blewitt G, Hammond WC, Kreemer C. 2018. Harnessing the gps data explosion for interdisciplinary science. *Eos* 99(10.1029).

Boehm J, Werl B, Schuh H. 2006. Troposphere mapping functions for gps and very long baseline interferometry from european centre for medium-range weather forecasts operational analysis data. *Journal of Geophysical Research: Solid Earth* 111(B2).

Boudin F, Bernard P, Meneses G, Vigny C, Olcay M, Tassara C, *et al.* 2021. Slow slip events precursory to the 2014 iquique earthquake, revisited with long-base tilt and gps records. *Geophysical Journal International*.

Brooks BA, Bevis M, Smalley R, Kendrick E, Manceda R, Lauría E, *et al.* 2003. Crustal motion in the southern Andes (26°–36°S): Do the Andes behave like a microplate? *Geochemistry, Geophysics, Geosystems* 4(10).

Cembrano J, Hervé F, Lavenu A. 1996. The liquiñe ofqui fault zone: a long-lived intra-arc fault system in southern chile. *Tectonophysics* 259(1-3): 55–66.

Chanard K, Fleitout L, Calais E, Rebischung P, Avouac J-P. 2018. Toward a global horizontal and vertical elastic load deformation model derived from grace and gnss station position time series. *Journal of Geophysical Research: Solid Earth* 123(4): 3225–3237.

Cifuentes IL. 1989. The 1960 Chilean earthquakes. *Journal of Geophysical Research: Solid Earth* 94(B1): 665–680.

Comte D, Eisenberg A, Lorca E, Pardo M, Ponce L, Saragoni R, *et al.* 1986. The 1985 central chile earthquake: A repeat of previous great earthquakes in the region? *Science* 233(4762): 449–453.

Comte D, Pardo M. 1991. Reappraisal of great historical earthquakes in the northern chile and southern peru seismic gaps. *Natural Hazards* 4(1): 23–44.

Dow J, Neilan R, Rizos C. 2009. The international GNSS service in a changing landscape of Global Navigation Satellite Systems. *Journal of Geodesy* 83(3-4): 191–198.

Dziewonski A, Chou T-A, Woodhouse JH. 1981. Determination of earthquake source parameters from waveform data for studies of global and regional seismicity. *Journal of Geophysical Research: Solid Earth* 86(B4): 2825–2852.

Ekström G, Nettles M, Dziewon'ski, A. 2012. The global cmt project 2004–2010: Centroid-moment tensors for 13 017 earthquakes. *Physics of the Earth and Planetary Interiors* 200: 1–9.

Fu Y, Argus DF, Freymueller JT, Heflin MB. 2013. Horizontal motion in elastic response to seasonal loading of rain water in the amazon basin and monsoon water in southeast asia observed by gps and inferred from grace. *Geophysical Research Letters* 40(23): 6048–6053.

Gobron K, Rebischung P, Van Camp M, Demoulin A, de Viron O. 2021. Influence of aperiodic non-tidal atmospheric and oceanic loading deformations on the stochastic properties of global gnss

vertical land motion time series. *Journal of Geophysical Research: Solid Earth* 126(9): e2021JB022370.

Herring T, King R, McClusky SC. 2010a. GAMIT: GPS Analysis at MIT, release 10.4.

Herring T, King R, McClusky SC. 2010b. GLOBK: Global Kalman filter VLBI and GPS analysis program release 10.4.

Hu Y, Bürgmann R, Uchida N, Banerjee P, Freymueller JT. 2016. Stress-driven relaxation of heterogeneous upper mantle and time-dependent afterslip following the 2011 tohoku earthquake. *Journal of Geophysical Research: Solid Earth* 121(1): 385–411.

Kendrick E, Bevis M, Smalley R, Brooks B. 2001. An integrated crustal velocity field for the central Andes. *Geochemistry, Geophysics, Geosystems* 2(11): n/a–n/a.

Kendrick E, Bevis M, Smalley R, Brooks B, Vargas RB, Laura E, *et al.* 2003. The nazca-south america euler vector and its rate of change. *Journal of South American Earth Sciences* 16(2): 125–131.

Khazaradze G, Wang K, Klotz J, Hu Y, He J. 2002. Prolonged post-seismic deformation of the 1960 great Chile earthquake and implications for mantle rheology. *Geophysical Research Letters* 29(22).

Klein E, Duputel Z, Zigone D, Vigny C, Boy J-P, Doubre C, *et al.* 2018. Deep transient slow slip detected by survey gps in the region of atacama, chile. *Geophysical research letters* 45(22): 12–263.

Klein E, Fleitout L, Vigny C, Garaud J. 2016. Afterslip and viscoelastic relaxation model inferred from the large scale postseismic deformation following the 2010 Mw 8.8 Maule earthquake (Chile). *Geophysical Journal International* 205(3): 1455–1472.

Klein E, Potin B, Pasten-Araya F, Tissandier R, Azua K, Duputel Z, *et al.* 2021. Interplay of seismic and a-seismic deformation during the 2020 sequence of atacama, chile. *Earth and Planetary Science Letters* 570: 117081.

Klein E, Vigny C, Fleitout L, Grandin R, Jolivet R, Rivera E, *et al.* 2017. A comprehensive analysis of the 2015 Mw 8.3 Illapel Earthquake from GPS and InSAR data. *Earth and Planetary Science Letters* 469: 123–134.

Klotz J, Khazaradze G, Angermann D, Reigber C, Perdomo R, Cifuentes O. 2001. Earthquake cycle dominates contemporary crustal deformation in central and southern Andes. *Earth and Planetary Science Letters* 193(3): 437–446.

Larson K, Freymuller J, Philipsen S. 1997. Global consistent rigid plate velocities from GPS. *J. Geophys. Res.* 102: 9961–9981.

Lomnitz C. 2004. Major earthquakes of Chile: A historical survey, 1535–1960. *Seismological Research Letters* 75: 368–378.

McCann W, Nishenko S, Sykes L, Krause J. 1979. Seismic gaps and plate tectonics: Seismic potential for major boundaries. *Pure and Applied Geophysics* 117: 1082–1147.

Métois M, Vigny C, Socquet A. 2012. Interseismic coupling, segmentation and mechanical behavior of the central Chile subduction zone. *Journal of Geophysical Research* 662: 120–131.

Métois M, Vigny C, Socquet A. 2016. Interseismic coupling, megathrust earthquakes and seismic swarms along the Chilean subduction zone (38°S–18°S). *Pure and Applied Geophysics* 173 (5): 1431–1449.

Moreno M, Melnick D, Rosenau M, Bolte J, Klotz J, Echtler H, *et al.* 2011. Heterogeneous plate locking in the south-central Chile subduction zone: Building up the next great earthquake. *Earth and Planetary Science Letters* 305.

Moreno M, Rosenau M, Oncken O. 2010. 2010 Maule earthquake slip correlates with pre-seismic locking of Andean subduction zone. *Nature* 467(7312): 198–202.

Nikolaidis R. 2002. *Observation of geodetic and seismic deformation with the Global Positioning System*. PhD thesis, University of California San Diego, La Jolla, CA.

Norabuena EO, Dixon TH, Stein S, Harrison CG. 1999. Decelerating nazca-south america and nazca-pacific plate motions. *Geophysical Research Letters* 26(22): 3405–3408.

Piñón DA, Gómez DD, Smalley Jr R, Cimbaro SR, Laura EA, Bevis MG. 2018. The history, state, and future of the Argentine continuous satellite monitoring network and its contributions to geodesy in Latin America. *Seismological Research Letters* 89(2A): 475–482.

Pritchard ME, Simons M. 2006. An aseismic slip pulse in northern Chile and along-strike variations in seismogenic behavior. *Journal of Geophysical Research* 1–14.

Rebischung P. 2021. Terrestrial frame solutions from the igs third reprocessing. In: *EGU General Assembly Conference Abstracts*, pp. EGU21–2144.

Rebischung P, Villiger A, Herring T, Moore M. 2019. Preliminary results from the third igs reprocessing campaign. In: *AGU Fall Meeting Abstracts*, vol. 2019, pp. G11A–03.

Ruegg J, Campos J, Madariaga R, Kausel E, De Chabalier J, Armijo R, *et al.* 2002. Interseismic strain accumulation in south central chile from gps measurements, 1996–1999. *Geophysical Research Letters* 29(11): 12–1.

Ruiz S, Aden-Antoniow F, Baez J, Otarola C, Potin B, Campo F, *et al.* 2017. Nucleation phase and dynamic inversion of the Mw 6.9 Valparaso 2017 earthquake in Central Chile. *Geophysical Research Letters* 44(20).

Ruiz S, Madariaga R. 2018. Historical and recent large megathrust earthquakes in chile. *Tectonophysics*.

Ruiz S, Metois M, Fuenzalida A, Ruiz J, Leyton F, Grandin R, *et al.* 2014. Intense foreshocks and a slow slip event preceded the 2014 Iquique Mw 8.1 earthquake. *Science* 345(6201): 1165–1169.

Schurr B, Asch G, Hainzl S, Bedford J, Hoechner A, Palo M, *et al.* 2014. Gradual unlocking of plate boundary controlled initiation of the 2014 Iquique earthquake. *Nature*.

Silverii F, D'Agostino N, Métois M, Fiorillo F, Ventafridda G. 2016. Transient deformation of karst aquifers due to seasonal and multiyear groundwater variations observed by GPS in southern Apennines (Italy). *Journal of Geophysical Research: Solid Earth* 121(11): 8315–8337.

Socquet A, Valdes JP, Jara J, Cotton F, Walpersdorf A, Cotte N, *et al.* 2017. An 8 month slow slip event triggers progressive nucleation of the 2014 Chile megathrust. *Geophysical Research Letters* 44(9): 4046–4053.

Suito H, Freymueller JT. 2009. A viscoelastic and afterslip postseismic deformation model for the 1964 Alaska earthquake. *Journal of Geophysical Research: Solid Earth* 114(B11): n/a–n/a.

Tilmann F, Zhang Y, Moreno M, Saul J, Eckelmann F, Palo M, *et al.* 2016. The 2015 illapel earthquake, central chile: A type case for a characteristic earthquake? *Geophysical Research Letters* 43(2): 574–583.

Trubienko O, Fleitout L, Garaud J-D, Vigny C. 2013. Interpretation of interseismic deformations and the seismic cycle associated with large subduction earthquakes. *Tectonophysics* 589(0): 126–141.

Trubienko O, Garaud J-D, Fleitout L. 2014. Models of postseismic deformation after megaearthquakes: the role of various rheological and geometrical parameters of the subduction zone. *Solid Earth Discussions* 6(1): 427–466.

Vigny C, Socquet A, Peyrat S, Ruegg J-C, Metois M, Madariaga R, *et al.* 2011. The 2010 Mw 8.8 Maule megathrust earthquake of central Chile, monitored by GPS. *Science* 332(6036): 1417–1421.

Williams SD, Bock Y, Fang P, Jamason P, Nikolaidis RM, Prawirodirdjo L, *et al.* 2004. Error analysis of continuous gps position time series. *Journal of Geophysical Research: Solid Earth* 109(B3).

Willis B. 1929. Studies in Comparative Seismology: Earthquake Conditions in Chile. Number 382. Carnegie Institution of Washington.

Yuzariyadi M, Heki K. 2021. Enhancement of interplate coupling in adjacent segments after recent megathrust earthquakes. *Tectonophysics* 801: 228719.

Zumberge J, Heflin M, Jefferson D, Watkins M, Webb F. 1997. Precise point positioning for the efficient and robust analysis of gps data from large networks. *Journal of Geophysical Research: Solid Earth* 102(B3): 5005–5017.

Cite this article as: Emilie Klein, Christophe Vigny, Jean-Mathieu Nocquet, Hugo Boulze. 2022. A 20 year-long GNSS solution across South-America with focus in Chile, *BSGF - Earth Sciences Bulletin* 193: 5.